



3D-printed polarization-independent low-cost flexible frequency selective surface based dual-band microwave absorber

Gaurav Chaitanya^{1,2} , Paritosh Peshwe¹, Saptarshi Ghosh³  and Ashwin Kothari⁴

Research Paper

Cite this article: Chaitanya G, Peshwe P, Ghosh S, Kothari A (2024) 3D-printed polarization-independent low-cost flexible frequency selective surface based dual-band microwave absorber. *International Journal of Microwave and Wireless Technologies*, 1–10. <https://doi.org/10.1017/S1759078724000692>

Received: 11 February 2024

Revised: 25 May 2024

Accepted: 10 June 2024

Keywords:

3D-printing; absorber; conformal; dual-band; frequency selective surface (FSS)

Corresponding author: Gaurav Chaitanya;
Email: chaitanya.gaurav@gmail.com

¹Department of Electronics and Communication Engineering, Indian Institute of Information Technology, Nagpur, India; ²Department of Electronics and Communications Engineering, Acropolis Institute of Technology and Research, Indore, India; ³Department of Electrical Engineering, Indian Institute of Technology Indore, Madhya Pradesh, Indore, India and ⁴Department of Electronics and Communication Engineering, Visvesvaraya National Institute of Technology, Nagpur, India

Abstract

A 3D-printed polarization-independent low-cost lightweight and flexible frequency selective surface based dual-band microwave absorber is presented in this paper. Two concentric square loops fabricated at different heights using 3D printing technology are responsible for exhibiting dual-band responses at 3.32 GHz (S-band) and 5.46 GHz (C-band) with more than 97% absorptivities. The corresponding full widths at half maximum bandwidths are observed as 230 MHz (3.21–3.44 GHz) and 450 MHz (5.27–5.72 GHz). The proposed topology is polarization-insensitive owing to the four-fold symmetry. The absorption phenomenon is explained with the analysis of current distributions at the surface and impedance curves at the frequencies of resonance. Further, the performance has been evaluated for both planar and curved surfaces with different angles of curvature, and the good agreement between the measured and simulated responses confirms the flexible behavior of the proposed structure.

Introduction

Recent technological advancements in communication systems at microwave, millimeter, and optical frequencies demand the design and development of multifarious devices. Frequency selective surfaces (FSSs) have evolved as one of the most researched fields to meet the standards of modern and advanced communication systems. FSS-based absorbers have a wide variety of applications in stealth technology [1], electromagnetic (EM) shielding [2], radar cross section reduction [3], EM energy harvesting [4], and so forth. Most of the reported FSS-based absorbers are designed on rigid, inflexible, and hard substrate materials, whereas real-world applications like military aircrafts [5], fighter jets [6], torpedoes [7], radars [8], missiles [9], wearable functional devices [10], RF sensors, bio-interfaces [11], shielding human and vehicles from battlefield radars [12], etc. involve curved or nonplanar surfaces. Therefore, developing a flexible, polarization-independent, lightweight, and cost-effective absorber for applications, which demand curvilinear surfaces and conformal designs, is the need of time.

Various types of flexible substrates have been utilized by the researchers to realize the conformal behavior of the absorbers, like PET (Polyethylene terephthalate) [13, 14], Silicon rubber [15], PDMS (Polydimethylsiloxane) [16], PVC (Polyvinyl chloride) [17], textile [12, 18], polyimide [19] and paper [20]. Few absorber geometries have been constructed by using ultrathin substrates, like Taconic [21], RT Duroid 5880 [22, 23], and FR4 [7, 24, 25] where the structures can be bent upto certain angles due to their low profiles. While they offer effective flexural strength, they are not ideal for applications involving prolonged and repetitive bending. Similarly, multi-layered geometries have been reported [26, 27]. Graphene and other composites have also been attempted to design flexible absorbers in [28]. However, it is very difficult to achieve flexibility while maintaining absorptivity in those types of design configurations. Further, their fabrication procedures are complex and expensive. In [29] absorber fabricated on a polyimide material using a complex laser ablation technique is presented. Additionally, a dual-layer triple-band flexible absorber was proposed on neoprene rubber, incorporating copper foil tape as a conductor [30]. However, due to the manual fabrication process, scaling up for large-scale applications presents significant challenges.

In this paper, a 3D-printed low-cost, lightweight, and conformal FSS-based absorber is designed and developed. Two concentric square loops are fabricated at different heights utilizing

the 3D printing technology to realize the dual-band absorption at two different frequency bands (S and C-bands). Owing to the use of the perforated topology, the geometry is flexible and can be bent to different curvatures, thereby satisfying the conformal behavior. The square loops have also been made at different heights, thus adding another degree of freedom to the design, unlike the fixed-height planar structures. The absorption mechanism is explained with the help of impedance curves and surface current distributions. The prototype of the presented absorber has also been built and its absorptivity responses are measured for leveled and bent surfaces, which concur with the simulated results.

Design and analysis

Unit cell response

Figure 1 illustrates the unit cell configuration consisting of two concentric square loops with different heights resonating at two different frequencies. The square loops are elevated on a base layer with 0.3 mm thickness ($H1$). The concentric square loops have heights of 1 mm ($H2$) and 1.5 mm ($H3$) for the outer loop and inner loop, respectively. The 3D printer-compatible filament

PLA (polylactic acid) substrate is used as the constituent dielectric (marked by grey color) with a dielectric constant of 2.1 and a loss tangent of 0.07. The metal ground plane at the back side of the structure and the conducting surfaces on the top of the square loops are considered copper metal with thicknesses of 0.065 mm each. The master-slave boundary conditions in the x-y axes and Floquet port excitation in the z-axis have been applied around the unit cell to analyze the structure for an infinite unit cell arrangement.

Figure 2 shows the reflectivity and absorptivity responses of the presented structure. The design exhibits a dual-band response having resonances at 3.32 GHz (S-band) and 5.46 GHz (C-band) with reflectivities of -20 dB and -15 dB, respectively, which correspond to absorptivities of 99% and 97%, respectively. This indicates that only 1% and 3% of incident EM wave are accounted as reflection loss at first and second frequencies, respectively. The corresponding full widths at half maximum bandwidths are observed as 230 MHz (3.21–3.44 GHz) and 450 MHz (5.27–5.72 GHz). The individual impacts of each loop have been studied in Fig. 3. It is clearly observed that the inner loop (design-I) contributes toward the second band resonating at 5.46 GHz and the outer loop (design-II) contributes toward the first band resonating at 3.32 GHz.

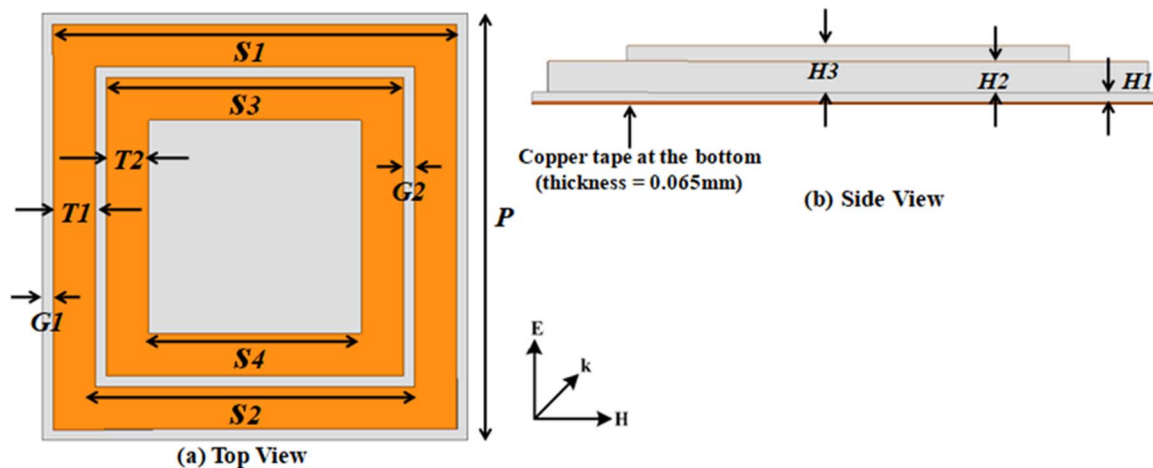


Figure 1. Proposed unit cell design $P = 20$ mm, $S1 = 19$ mm, $S2 = 15$ mm, $S3 = 14$ mm, $S4 = 10$ mm, $T1 = 2$ mm, $T2 = 2$ mm, $G1 = 0.5$ mm, $G2 = 0.5$ mm, $H1 = 0.3$ mm, $H2 = 1$ mm, $H3 = 1.5$ mm.

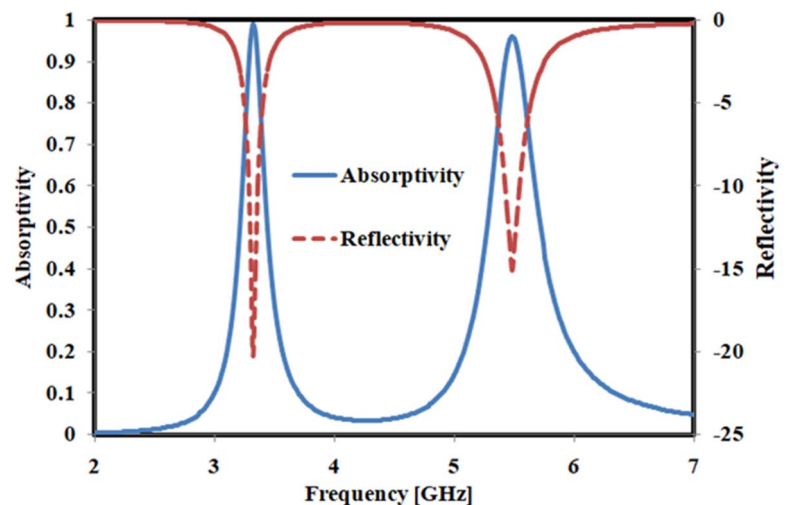


Figure 2. Absorptivity and reflectivity curves of the proposed dual-band absorber.

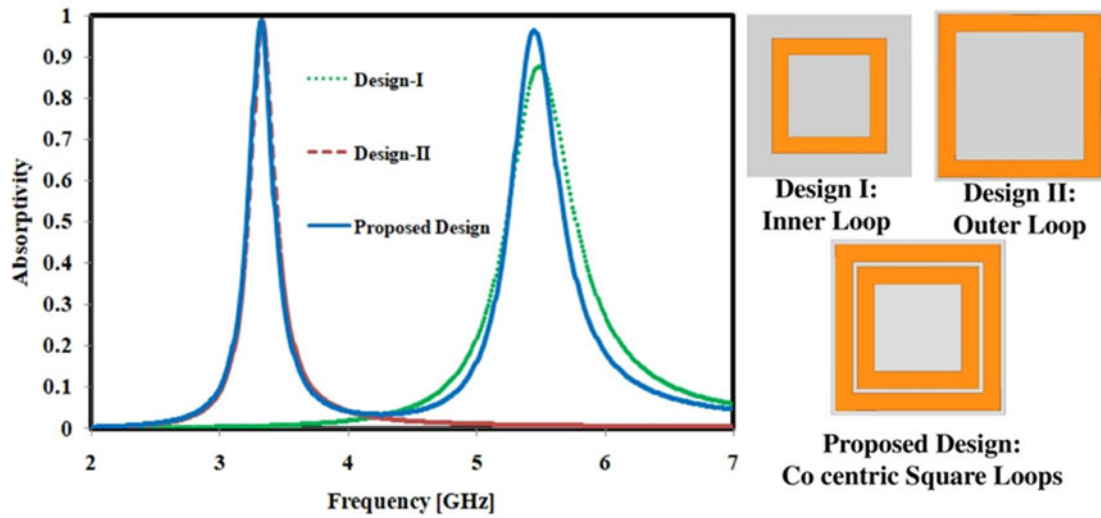


Figure 3. Effect of individual square loop designs on absorptivity curves.

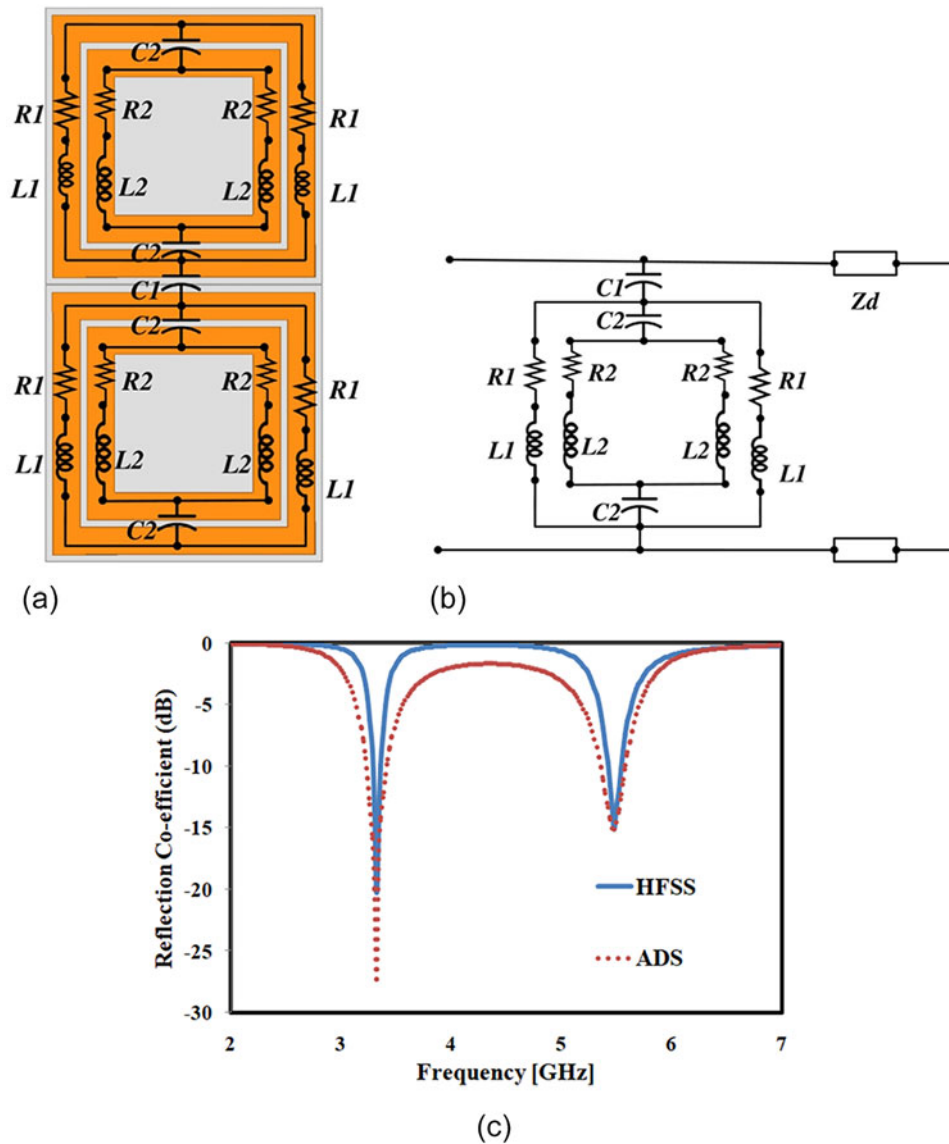


Figure 4. Equivalent circuit model of the proposed absorber: (a) contribution of individual segments, (b) overall circuit model, and (c) comparison of equivalent circuit model response and simulated result of the absorber.

Equivalent circuit model

The equivalent circuit model of the presented structure is illustrated in Fig. 4. $L1$ and $L2$ are the effective inductances corresponding to the lengths of the outer and inner square loops, respectively. $R1$ and $R2$ are resistances due to the finite conductivity of the top copper metal of the loops and represent small ohmic losses. $C1$ represents the equivalent capacitance between the adjacent unit cells; whereas $C2$ shows the capacitance between the inner and outer loops of the unit cell. The dielectric substrate is represented by a transmission line, and the bottom metal plane can be considered a short circuit. This shorted circuit transmission line is represented by an equivalent inductance Z_d . Thus, the total impedance (Z_{total}) of the presented structure can be calculated as

$$Z_{total} = Z_i || Z_o || Z_d \quad (1)$$

where Z_i is the equivalent impedance of the inner loop (a combination of $R2$, $L2$, and $C2$) and Z_o is the equivalent impedance of the outer loop (a combination of $R1$, $L1$, and $C1$). By regulating different geometric dimensions of each of the square loops as well as the substrate properties, their corresponding impedances can be controlled, and resonances can be generated accordingly.

The Advanced Design System software is used to determine the values of the circuit parameters of the equivalent circuit model. After optimization, the determined values are as follows: $R1 = 7.68 \Omega$, $L1 = 1.01 \text{ nH}$, $C1 = 0.78 \text{ pF}$, $R2 = 1.96 \Omega$, $L2 = 1.98 \text{ nH}$, and $C2 = 0.2 \text{ pF}$. The comparison curves, showing the reflectivity responses evaluated from the calculated results of the equivalent circuit model and those from the simulation software High Frequency Structure Simulator (HFSS) Version 14.0, are depicted in Fig. 4(c). It is clearly evident that both curves exhibit significant alignment, thereby validating the correctness of the proposed equivalent circuit model.

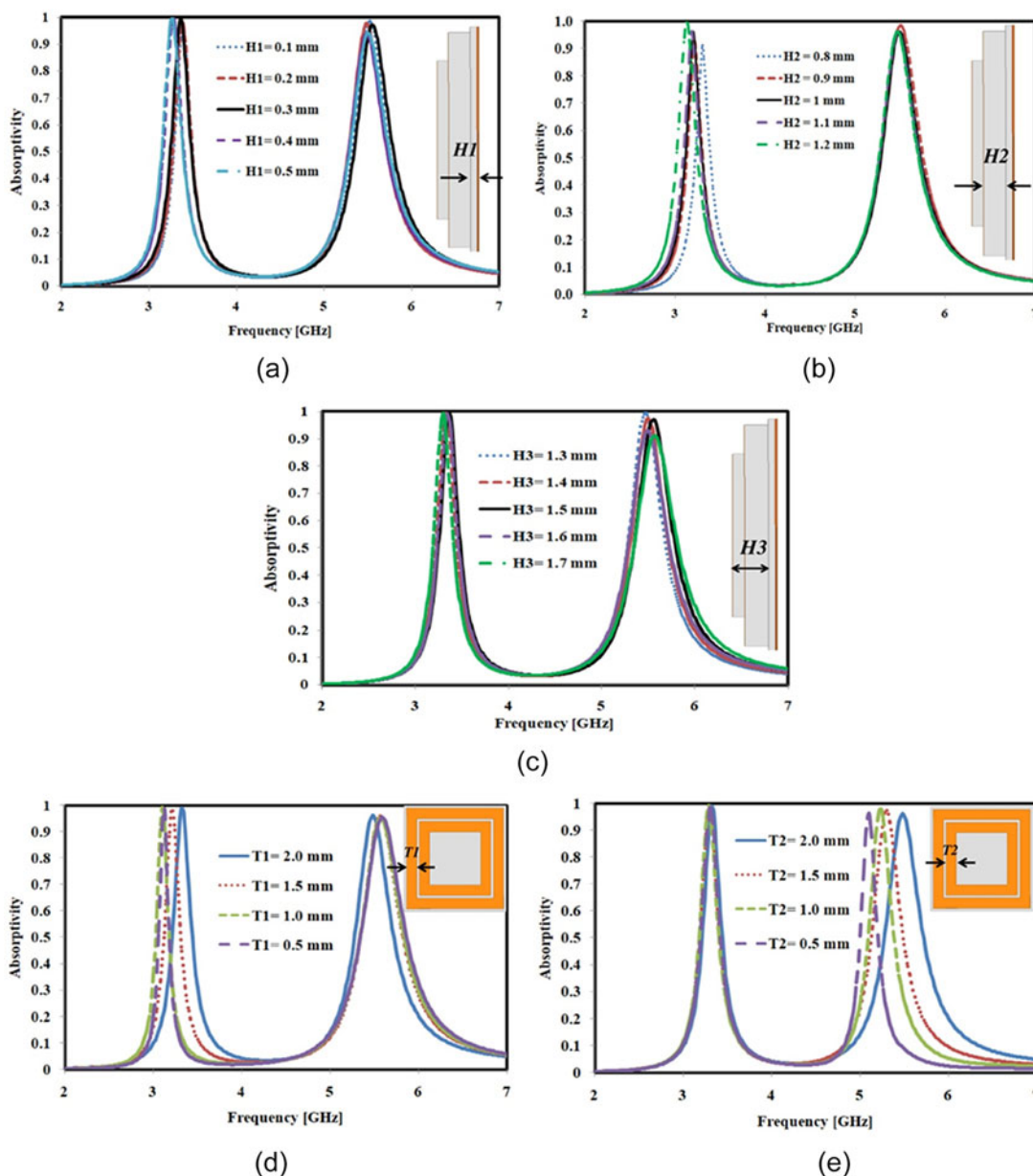


Figure 5. Study of variation in design parameters on the absorptivity responses: (a) $H1$, (b) $H2$, (c) $H3$, (d) $T1$, and (e) $T2$.

Parametric analysis

The effects of variation in different design parameters are studied and illustrated in Fig. 5(a–e). Figure 5(a) depicts the variation of the base substrate height $H1$, which shows that both absorption peaks are shifted marginally. This base substrate is used for the support during fabrication, and hence is kept as minimal as possible ($= 0.3$ mm). Owing to the advantage of 3D printing technology, the heights of each of the square loops can be realized with different values, and therefore, their variations are analyzed individually. Figure 5(b) represents that with the increase in the height of the outer square loop ($H2$), a slight shift in the resonance frequency is observed in the lower band, whereas the higher band remains constant.

While varying the height of the inner square loop ($H3$), the change in the absorption frequency of the higher band is more prominent than that of the lower band, as observed in Fig. 5(c). Figure 5(d) and (e) represent the variation in the width of the outer loop ($T1$) and inner loop ($T2$), respectively. It is observed that the corresponding resonance frequencies shift toward the lower side with the decrease in the widths. The inductances are increased with smaller values of metallic widths that cause the redshift of the absorption bands.

Impedance graph

One of the important parameters that should be investigated in absorber geometry is its input impedance. Since the proposed structure is terminated with a metal ground, there is no transmission ($S_{21} = 0$), and the absorptivity can be determined from the reflection coefficient (S_{11}) only. A near-unity absorption response can be obtained, if the input impedance (Z_{in}) of the geometry can be matched with the free space impedance (377Ω). The real and imaginary parts of the input impedance of the proposed absorber are illustrated in Fig. 6, which is determined using Equation 2. The values of real and imaginary impedances obtained at resonant frequencies are tabulated in Table 1. It is observed that the maximum absorption is perceived at the resonant frequencies as the real part of Z_{in} is close to unity and its imaginary part is close to zero.

$$Z_{in} = \sqrt{\frac{(1 + S_{11})^2 - (S_{21})^2}{(1 - S_{11})^2 - (S_{21})^2}} \quad (2)$$

Surface current and electric field distribution

The absorption mechanism has further been examined by analyzing the surface current and electric field distributions of the proposed design at two resonant frequencies (3.32 GHz and 5.46 GHz), as illustrated in Fig. 7. The concentration of surface current is observed at the inner loop at 5.46 GHz and the outer loop at 3.32 GHz with anti-parallel orientation on the top and bottom layers of the structure, thus producing the magnetic field excitation formed due to the accumulation of circulating current. The electric field excitations are mostly observed in the metallic patches. At resonance frequencies, both magnetic and electric fields excite at the same time and achieve the maximum absorptivity.

Polarization and oblique incidence angle variation

The absorption responses under different polarization angles (ϕ) of the proposed design is depicted in Fig. 8(a). This study is carried out for a constant incident EM wave vector direction, while

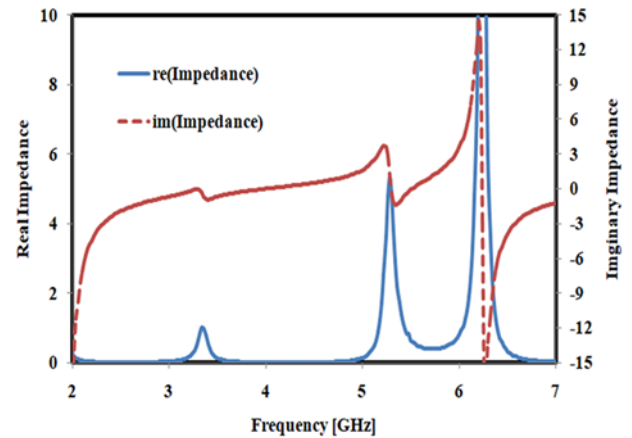


Figure 6. Real and imaginary impedance curves.

Table 1. Values of real and imaginary impedances for the frequencies of resonances

Frequency [GHz]	Real (Z)	Imaginary (Z)
$f1 = 3.32$	0.85	-0.11
$f2 = 5.48$	0.83	-0.22

varying both magnetic and electric fields with an angle ranging from $\phi = 0$ degree to 90 degree with a step size of 15 degree. A similar absorption behavior is observed for all the cases, thus confirming the structure as polarization-independent. The impacts of the incident angle variation on the absorption characteristic under the transverse electric (TE) and transverse magnetic (TM) polarization cases are investigated in Fig. 8(b) and (c), respectively. With a steady direction of the electric field, while varying the incident angle (θ) of the magnetic field and direction of wave propagation, the TE mode is analyzed. Alternatively, with a steady direction of the magnetic field, while varying the incident angle (θ) of the electric field and direction of wave propagation, the TM mode is analyzed. For both cases, the absorption magnitudes have been observed to remain almost constant up to 45 degree incident angle, but a decrease in the absorption magnitude is observed with a further increase in the angle of incidence. As a result, it has been concluded that stable absorption responses are maintained up to a 45-degree angle for both TE and TM modes in both absorption bands.

Conformal analysis

The conformal behavior of the proposed design is investigated by bending the structure on various 3D printed cylindrical mockup models having angles of curvature at 180 degree, 135 degree, 90 degree, and 0 degree, as depicted in Fig. 9(a). With the increase in the arc angle, the radius of curvature (ROC) decreases; thus, the flat surface has the radius maximum (infinity) and the 180 degree curvature has the radius minimum. The absorption behavior of the proposed design is simulated for different arc angles and it is observed in Fig. 9(b) that the response remains relatively stable with a slight frequency shift with the decrease in the angle. It is worth noting that owing to the use of 3D printing technology, the proposed geometry can be wrapped on different cylindrical surfaces even though the total height of the structure is 1.8 mm

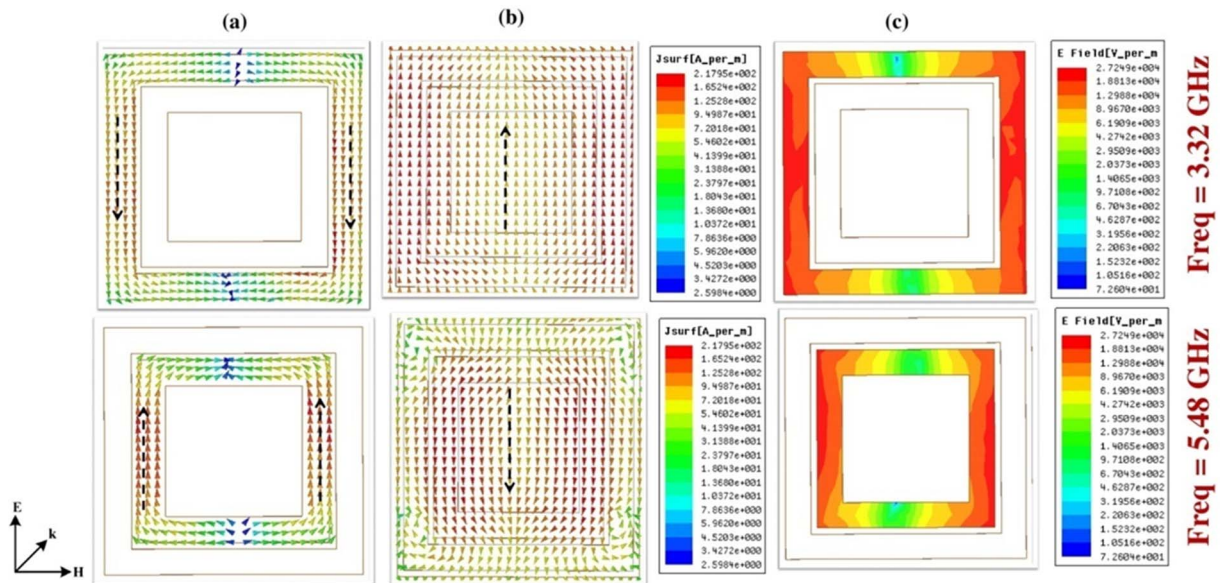


Figure 7. Surface current distribution at (a) top surface, (b) bottom surface, and (c) electric field distribution at two different absorption peaks.

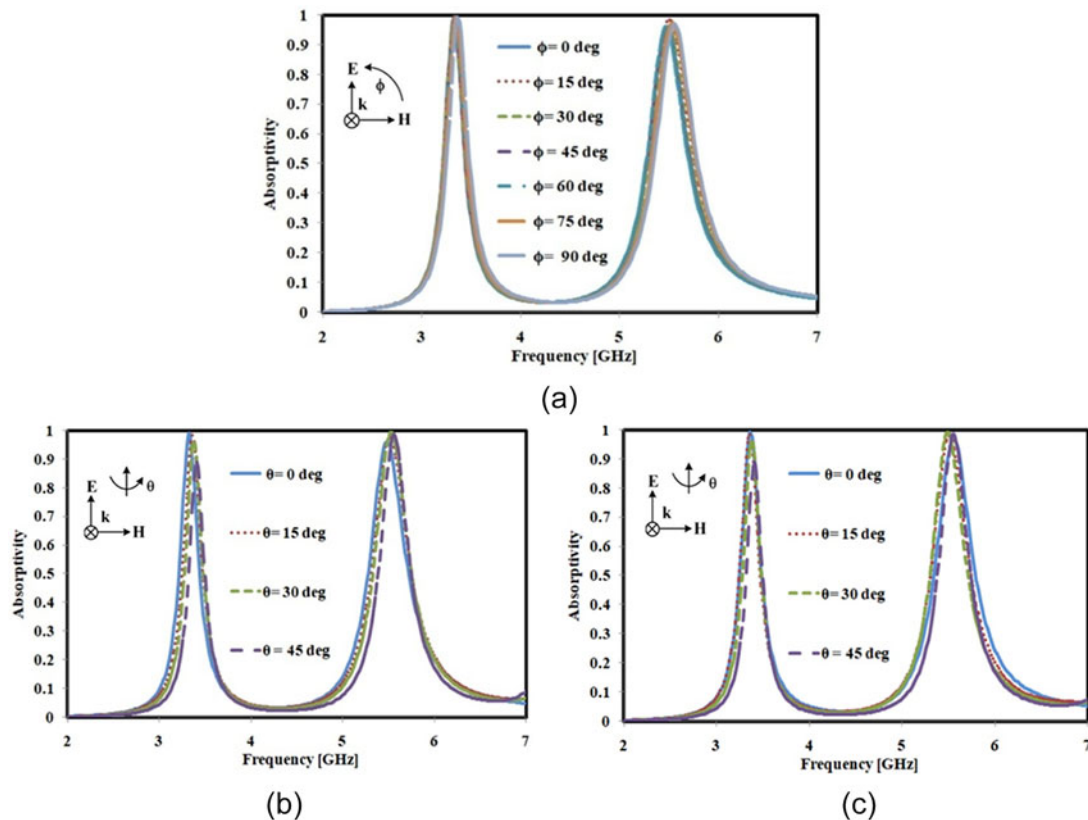


Figure 8. Simulated absorptivity patterns (a) at different angles of polarization (ϕ), and at varied angles of incidence (θ) under (b) TE polarization, and (c) TM polarization.

($H1 + H3 = 0.3 \text{ mm} + 1.5 \text{ mm}$), which is a comparatively larger thickness to be bent.

Fabrication and measurement results

Figure 10(a) shows the proposed absorber design fabricated using 3D printing technology with a 12×12 unit cell arrangement having

a total size of $240 \times 240 \text{ mm}^2$. Commercially available PLA filament is used for the fabrication of the substrate pattern using the Pratham 6.0 3D printer by Make3D.in. Different heights have been realized for different square loops on the top of the base substrate using a single-step fabrication. Afterward, the back side ground and top conducting surface are realized using 0.065 mm thick adhesive copper tape. The patterns have been cut from the copper

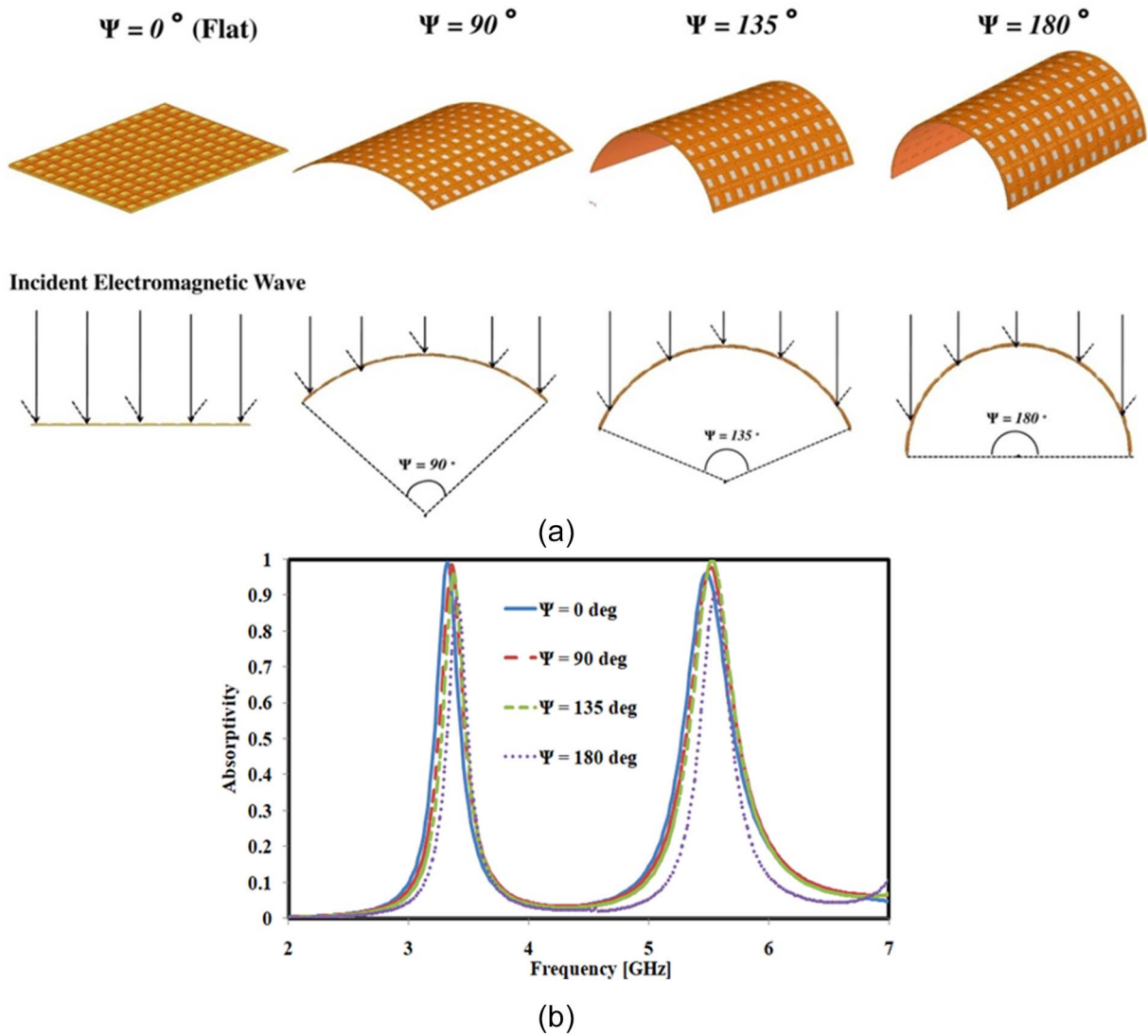


Figure 9. (a) EM wave incidence on different ROC on which the absorber structure is wrapped, (b) simulated absorptivity responses for different ROC values.

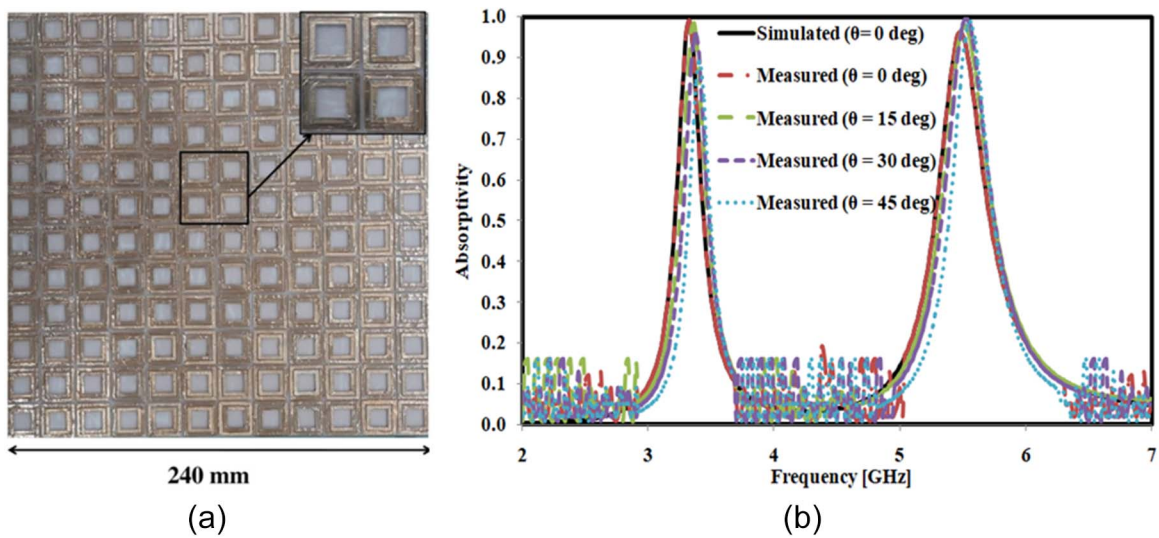


Figure 10. (a) Fabricated prototype of 3D printed dual-band absorber. (b) Simulated and measured responses of the presented absorber.

tape using a Skycut C24 vinyl cutter and pasted on the 3D printed substrate accurately.

The conventional free space method has been employed for the measurement comprising an assembly of two horn antennas connected to a handheld Anritsu vector network analyzer. The prototype has been mounted in the middle of an absorbing wall, where the antennas are placed on the same side of the structure in close proximity. The reflection response is first measured for a copper plate of identical dimensions and then it is replaced with the original prototype. The difference in reflection between the original prototype and that of the copper plate gives the real reflection coefficient (or absorption). Figure 10(b) shows the comparative analysis of the simulated and measured absorption responses, and they concur well with each other except for minor undulation due to size limitation and fabrication imprecision. The bending analysis has also been studied by wrapping the structure on mock-up cylindrical models having different arc angles as shown in Fig. 11(a). Stable absorption responses

are observed for different radii of curvature, as illustrated in Fig. 11(b).

A comparison of the absorber presented in this study with flexible absorbers from prior research is outlined in Table 2. The analysis reveals that despite its relatively large thickness, the presented absorber maintains conformality due to its perforated topology. Additionally, the absorber's resonators are constructed at varying heights, providing an additional level of design flexibility not found in fixed-height planar structures having resonators on same level.

Conclusion

A 3D-printed polarization-insensitive low-cost lightweight and flexible FSS-based dual-band absorber is presented. Two concentric square loops with different substrate heights are designed for exhibiting dual-band responses at 3.32 GHz and 5.46 GHz resonating in S and C bands, respectively, with more than 97%

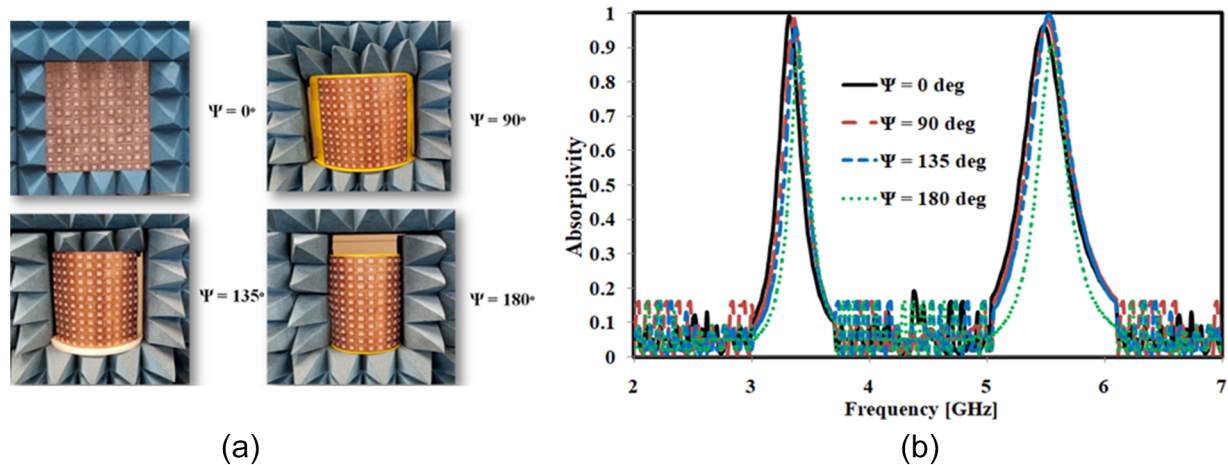


Figure 11. (a) Measurement setup of the fabricated prototype wrapped on mockup models having different radii of curvature. (b) Measured absorptivity responses corresponding to different models.

Table 2. Comparative study of the proposed absorber with respect to existing literature on flexible microwave absorbers

Absorber	Thickness	Unit cell size	Flexible	Polarization independent	Fabrication method	Substrate material	Number of resonance	Resonators at different heights
Presented	(1.8 mm) 0.020λ	0.22λ	Yes	Yes	3D printing	PLA	2	Yes
[24], 2023	(0.3 mm) 0.010λ	0.52λ	NR	Yes	PCB technology	FR4	3	No
[13], 2021	(0.32 mm) 0.006λ	0.23λ	Yes	Yes	PCB technology	PET	3	No
[29], 2020	(0.1 mm) 0.011λ	0.22λ	Yes	Yes	Laser ablation	Polymide	3	No
[25], 2019	(0.35 mm) 0.006λ	0.22λ	Yes	No	PCB technology	FR4	2	No
[7], 2019	(0.1 mm) 0.003λ	0.25λ	Yes	Yes	PCB technology	FR4	1	No
[14], 2019	(0.32 mm) 0.010λ	0.50λ	Yes	Yes	PCB technology	PET	2	No
[30], 2019	(3 mm) 0.037λ	0.20λ	Yes	Yes	Manual	Neoprene rubber	3	No

λ : Wavelength (= 90.36 mm) to lowest resonance frequency (3.32 GHz); NR = not reported.

absorptivities. The absorption behavior has been explained with the help of impedance graphs and surface current distributions. The prototype has also been fabricated and its absorptivity responses are measured for leveled and bent surfaces at different radii of curvature which concur with the simulated results, thereby confirming its flexible behavior.

Acknowledgements. The authors acknowledge the support of Applied Electromagnetic Laboratory of IIT Indore for providing testing and measurement facilities and AICTE IDEA Lab, Acropolis, Indore for fabrication resources.

Funding. This research received no external funding.

Competing interests. The authors declare that they have no known competing financial interests or personal relationships that could have appeared to influence the work reported in this paper.

References

- Priyanka SM, Alegaonkar PS and Baskey HB (2023) Design and manufacturing of a hexapattern frequency selective surface absorber for aerospace stealth application. *ACS Applied Materials & Interfaces* **15**(30), 37107–37115.
- Shukoor MA and Dey S (2023) Wideband reconfigurable multifunctional absorber/reflector with bandpass/bandstop filtering and band-notch absorption for RCS and EMI shielding. *IEEE Transactions on Electromagnetic Compatibility* **66**(1), 153–160.
- Das P and Mandal K (2021) Hybrid frequency selective surface phase cancelation structure based broadband switchable radar cross section reduction. *International Journal of RF and Microwave Computer-Aided Engineering* **31**(3), e22554.
- Amin M, Almoneef TS, Siddiqui O, Aldhaeabi MA and Mouine J (2021) An interference-based quadruple-L cross metasurface absorber for RF energy harvesting. *IEEE Antennas and Wireless Propagation Letters* **20**(10), 2043–2047.
- Zhang Y, Dong H, Mou N, Chen L, Rihong L and Zhang L (2020) High-performance broadband electromagnetic interference shielding optical window based on a metamaterial absorber. *Optics Express* **28**(18), 26836–26849.
- Hannan S, Tariqul Islam M, Soliman MS, Sahar NBM, Singh MSJ, Faruque MRI and Alzamil A (2022) A filling-factor engineered, perfect metamaterial absorber for multiple applications at frequencies set by IEEE in C and X bands. *Journal of Materials Research and Technology* **19**, 934–946.
- Chejarla S, Thummaluru SR and Chaudhary RK (2019) Flexible metamaterial absorber with wide incident angle insensitivity for conformal applications. *Electronics Letters* **55**(3), 133–134.
- Kang J, Zeng Q, Duan J, Jing H, Hao J, Song C, Wang J and Zhang B (2023) Multispectral flexible ultrawideband metamaterial absorbers for radar stealth and visible light transparency. *Optical Materials* **135**, 113351.
- Zhou Y, Qin Z, Liang Z, Meng D, Xu H, Smith DR and Liu Y (2021) Ultra-broadband metamaterial absorbers from long to very long infrared regime. *Light: Science & Applications* **10**(1), 138.
- Gong P, Hao L, Li Y, Li Z and Xiong W (2021) 3D-printed carbon fiber/polyamide-based flexible honeycomb structural absorber for multifunctional broadband microwave absorption. *Carbon* **185**, 272–281.
- Wang Y, Zhao C, Wang J, Luo X, Xie L, Zhan S, Kim J, Wang X, Liu X and Ying Y (2021) Wearable plasmonic-metasurface sensor for noninvasive and universal molecular fingerprint detection on biointerfaces. *Science Advances* **7**(4), eabe4553.
- Gaganpreet S, Sheokand H, Chaudhary K, Srivastava KV, Ramkumar J and Ramakrishna SA (2019) Fabrication of a non-wettable wearable textile-based metamaterial microwave absorber. *Journal of Physics D Applied Physics* **52**(38), 385304.
- Kalraiya S, Kumar Chaudhary R and Kumar Gangwar R (2021) Polarization independent triple band ultrathin conformal metamaterial absorber for C-and X-frequency bands. *AEU-International Journal of Electronics and Communications* **135**, 153752.
- Kalraiya S, Chaudhary RK, Abdalla MA and Gangwar RK (2019) Polarisation independent dual-band conformal metamaterial absorber for x-band microwave application. *Electronics Letters* **55**(9), 546–548.
- Weimei L, Jin H, Zeng Z, Zhang L, Zhang H and Zhang Z (2017) Flexible and easy-to-tune broadband electromagnetic wave absorber based on carbon resistive film sandwiched by silicon rubber/multi-walled carbon nanotube composites. *Carbon* **121**, 544–551.
- Jeong H and Lim S (2017) A stretchable electromagnetic absorber fabricated using screen printing technology. *Sensors* **17**(5), 1175.
- Aqilaff N, TeguhYudistira H and Qalbina F (2023) Design of tripartite square ring metamaterial absorber using polyvinyl chloride as a flexible substrate at s-band and c-band spectrums. *Journal of Materials Science: Materials in Electronics* **34**(3), 199.
- Lee D, Ki Kim H and Lim S (2017) Textile metamaterial absorber using screen printed channel logo. *Microwave and Optical Technology Letters* **59**(6), 1424–1427.
- Deng G, Kun L, Sun H, Yang J, Yin Z, Li Y, Chi B and Li X (2020) An ultrathin, triple-band metamaterial absorber with wide-incident-angle stability for conformal applications at X and Ku frequency band. *Nanoscale Research Letters* **15**, 1–10.
- Tirkey MM and Gupta N (2021) Broadband polarization-insensitive inkjet-printed conformal metamaterial absorber. *IEEE Transactions on Electromagnetic Compatibility* **63**(6), 1829–1836.
- Zargar MM, Rajput A, Saurav K and Koul SK (2021) Single-layered flexible dual transmissive rasorbers with dual/triple absorption bands for conformal applications. *IEEE Access* **9**, 150426–150442.
- Joy V, Baghel S, Tabassum Nazeer S and Singh H (2023) Broadband, polarization-insensitive and ultra-thin metasurface-based radar-absorbing structure for radar cross-section reduction of planar/conformal hotspots. *Journal of Electronic Materials* **52**, 6625–6636.
- Luo GQ, Weiliang Y, Yufeng Y, Jin H, Fan K and Zhu F (2020) Broadband dual-polarized band-absorptive frequency-selective rasorber using absorptive transmission/reflection surface. *IEEE Transactions on Antennas and Propagation* **68**(12), 7969–7977.
- Chaitanya G, Peshwe P, Ghosh S and Kothari A (2023) Design of bandwidth-enhanced polarization controlled frequency selective surface based microwave absorber. *International Journal of Microwave and Wireless Technologies*, 1–9.
- Kalraiya S, Ameen M, Kumar Chaudhary R and Kumar Gangwar R (2019) Compact ultrathin conformal metamaterial dual-band absorber for curved surfaces. *International Journal of RF and Microwave Computer-Aided Engineering* **29**(12), e21929.
- Xia J, Wei J, Liu Y, Zhang Y, Guo S, Chengli L, Bie S and Jiang J (2020) Design of a wideband absorption frequency selective rasorber based on double lossy layers. *IEEE Transactions on Antennas and Propagation* **68**(7), 5718–5723.
- Hang Y, Wei J, Lin L, Liu F, Miao L, Bie S and Jiang J (2021) A frequency-selective surface rasorber based on four functional layers. *IEEE Transactions on Antennas and Propagation* **69**(5), 2768–2778.
- Anjali M, Rengaswamy K, Ukey A, Stephen L, Krishnamurthy CV and Subramanian V (2023) Flexible metamaterial based microwave absorber with epoxy/graphene nanoplatelets composite as substrate. *Journal of Applied Physics* **133**(6), 063105.
- Xin W, Binzhen Z, Wanjun W, Junlin W and Junping D (2017) Design, fabrication, and characterization of a flexible dual-band metamaterial absorber. *IEEE Photonics Journal* **9**(4), 1–12.
- Kaur KP, Upadhyaya T, Palandoken M and Gocen C (2019) Ultrathin dual-layer triple-band flexible microwave metamaterial absorber for energy harvesting applications. *International Journal of RF and Microwave Computer-Aided Engineering* **29**(1), e21646.



Gaurav Chaitanya earned his Bachelor's degree in Electronics & Communication Engineering in 2007 followed by a Master's degree from IES, IPS Academy, Indore (affiliated to RGPV, Bhopal, India) in 2012. He boasts over 17 years of teaching experience at the Acropolis Institute of Technology and Research, Indore, India. Currently, he pursues his doctoral research at the Indian Institute of Information Technology, Nagpur, India. He holds Senior Membership at IEEE and Life Membership at ISTE. His research interests encompass Frequency Selective Surfaces (FSS), Metamaterials, and Absorber design.

He holds Senior Membership at IEEE and Life Membership at ISTE. His research interests encompass Frequency Selective Surfaces (FSS), Metamaterials, and Absorber design.



Dr. Paritosh Peshwe completed his Master's degree in Microelectronics from BITS, Pilani in 2013, and attained his PhD in Antenna Design from VNIT, Nagpur in 2019. His expertise lies in Antenna Design and Wireless Communication. Currently, he serves as an Assistant Professor in the Department of Electronics and Communication Engineering at the Indian Institute of Information Technology, Nagpur, and is a member of IEEE.



Dr. Saptarshi Ghosh holds an MTech and PhD in Electrical Engineering from the Indian Institute of Technology, Kanpur, India, awarded in 2013 and 2017 respectively. He subsequently worked as a Postdoctoral Research Fellow at Chung-Ang University, Seoul, Korea, before joining the Indian Institute of Technology Indore, Madhya Pradesh, India, where he presently serves as an Associate Professor. His research expertise spans electromagnetics, frequency selective surfaces, reconfigurable circuits, and metasurfaces. Dr. Ghosh actively contributes as a referee for various IEEE Journals and Conferences, and he holds membership in IEEE and serves as an Associate Editor of IEEE Antennas and Wireless Propagation Letters.



Dr. Ashwin Kothari obtained his PhD from Visveswariya National Institute of Technology, Nagpur in 2010. His research interests include Communication, Signal processing, Rough Sets, Cognitive Radio, Antennas, and Embedded systems. Currently, he holds the position of Professor and Head in the Department of Electronics and Communication Engineering at VNIT, Nagpur. Additionally, he has served as an In Charge Dean at the Indian Institute of Information Technology, Nagpur.